

Short Communication

Fabrication of Ultrafine Amorphous Pd-Ni-P Nanoparticles Supported on Carbon Nanotubes as an Effective Catalyst for Electro-oxidation of Methanol

Ming Zhao*, Yuan Ji, and Ning Zhong

School of Chemical Engineering, China University of Mining and Technology, No1, Daxue Road, Xuzhou, 221116, P. R. China

*Email: ming815zhao@163.com

Received: 21 September 2016 / *Accepted:* 18 October 2016 / *Published:* 10 November 2016

We presented the fabrication of ultrafine amorphous Pd-Ni-P nanoparticles with a mean size of 3 nm. During the reduction, the use of borane *tert*-butylamine complex was crucial for the small particle formation. Notably, the addition of strong reducing reagent does not lead to the formation of crystallized Pd or Ni-P phases at all. The amorphous Pd-Ni-P composite was proved to be the most efficient catalyst in comparison with Pd, Pd-Ni, and even its crystalline counterpart for the electrochemical oxidation of methanol in alkaline medium. Moreover, compared with Vulcan XC-72, carbon nanotubes was found to be a more effective support with which 1.8 times high specific activity was achieved.

Keywords: palladium; amorphous materials; nanoparticles; carbon nanotube; electro-oxidation

1. INTRODUCTION

Direct methanol fuel cell is one type of proton exchange membrane fuel cell (PEMFC). This device was widely researched as a promising portable power as it is safe and provides clean energy. Platinum is commonly used to catalyze the oxidation of methanol, ethanol and formic acid etc. in the anode of a fuel cell. However, Pt takes high cost and is prone to suffer CO poisoning. On the other hand, palladium shows versatile catalytic properties[1-5] and accredited to be a best alternative to Pt as anode catalyst in PEMFC as it is less expensive and not subject to CO poisoning.[6-8] However, Pd is prone to be oxidized and dissolved and loss activity quickly in oxidation mediums.[9-11] Phosphorus bears abundant valence electrons which would affect the electronic states of metal elements to generate

significant effect on catalytic properties.[12-15] Recently, Li *et al.* reported Pt-Ni-P porous nanotube arrays with good performance for methanol oxidation reaction (MOR).[12] Hu *et al.* deposited Pd onto Ni₂P nanoparticles (NPs) to form a hybrid with excellent activity and stability in electro-oxidation of formic acid.[16] Zhang *et al.* synthesized three dimensional Pd-P NP networks.[17] Carbon nanotubes (CNTs) show exceptional chemical and physical properties such as high surface area, electrical conductivity, toughness, and so on, which were widely researched in electrochemical and electronic devices.[18] Fundamental and experimental studies were reported on the nature of the interaction between metal and surfaces of CNTs.[19] Metal-CNTs hybrids displayed versatile catalysis in fuel cell reactions.[20-23]

We have previously reported the fabrication of 8-17 nm amorphous Pd-Ni-P NPs.[24] X-ray photoelectron spectroscopy (XPS) revealed the existence of Pd-P covalent bond within the NPs, which results in the electron deficiency of Pd, which contributed to the effective and stable catalysis for MOR. To improve the utilization of noble metal (Pd) and the efficiency of catalyst, we aimed to produce much smaller Pd-Ni-P NPs with a size <5 nm. Borane-amine complex was an efficient reductant for the production of ultrafine metal NPs, and boron does not associate with Pd or Pt.[6] Herein, we chose borane *tert*-butylamine complex (BTB) as the co-reductant of oleylamine (OLA). We presented for the first time the fabrication of ultrafine amorphous Pd-Ni-P NPs (3 nm). The composite was proved to be the most efficient catalyst compared with Pd, Pd-Ni, and its crystalline counterpart for MOR. Compared to Vulcan XC-72, CNTs were a more suitable support, and the specific activity with Pd₂₅Ni₂₅P₅₀/CNTs reached up to 0.91 mA/cm²_{Pd}, which is 1.8 times as high as that of Pd₂₅Ni₂₅P₅₀/C (C represents Vulcan XC-72).

2. EXPERIMENTAL SECTION

Chemicals. Palladium (II) acetylacetonate (Pd(acac)₂, 99%), nickel (II) acetylacetonate (Ni(acac)₂, 95%), triphenylphosphine, ReagentPlus[®] (TPP, 99%), borane *tert*-butylamine complex (BTB, powder, 97%), trioctylphosphine oxide (TOPO, technical grade 90%), oleylamine (OLA, technical grade 70%), commercial Pd (30% Pd on carbon matrix), and nafion[®] perfluorinated ion-exchange resin (5 wt.% soln in lower aliphatic alcohols/H₂O mix contains 15-20% water) were purchased from Sigma-Aldrich Co.; carbon black (Vulcan XC-72) was purchased from Moubic INC; carbon nanotube multi-walled (60-100 nm diam., 1-2 um length) was purchased from Tokyo Chemical Industry Co., Ltd; polishing alumina (0.05 μm) was purchased from BAS Inc. All the reagents were used without further purification.

Characterizations. Scanning electron microscopy (SEM), transmission electron microscopy (TEM) and high resolution TEM (HRTEM) were performed on a JEOL JEM-2100 (HR) operated at 200 kV. Energy-dispersive X-ray (EDX) was performed on a JED-2300T. X-ray diffraction (XRD) was performed on a Rigaku RINT Ultima III.

Electrochemical experiments. Cyclic voltammogram (CV) experiments were performed using a three-electrode setup (Iviumstat electrochemical analyzer, Ivium Technologies). A conventional three-electrode cell was used, including an Hg/Hg₂Cl₂ (saturated KCl) electrode as an reference

electrode, a pure platinum sheet as counter electrode, and a modified glassy carbon electrode (GCE) (with a surface area of 0.196 cm^2 , BAS Inc.) as working electrode. For the electro-catalyst preparation, a solution of catalysts (2 mg) in nafion (0.01 mL), distilled H_2O (0.095 mL), and ethanol (0.095 mL) was under ultrasonic for 20 min to form an ink. The modified GCE was coated with the as-obtained catalyst ink and dried naturally at room temperature. The CV measurements for electrochemical surface areas were performed in N_2 -saturated 0.5 M KOH (aq.) at a scan rate of 50 mV s^{-1} at 298K. The CV experiments for methanol oxidation were performed in 0.5 M KOH (aq.) that contained 1.0 M methanol at a scan rate of 50 mV s^{-1} at 298K.

Material preparation. The ultrafine Pd-Ni-P NPs were synthesized via a one-pot solvothermal procedure[24]: palladium acetylacetonate (0.4 mmol), nickel acetylacetonate (0.4 mmol) and triphenylphosphine (1.76 mmol) as Pd, Ni, and P sources, respectively, trioctylphosphine oxide (TOPO, 6 mmol) as a surfactant, OLA (12 mL) as a reducing reagent as well as a stabilizer, and BTB (2 mmol) as a co-reductant. A mixture of the chemicals mentioned above was deaerated at $50 \text{ }^\circ\text{C}$, stirred at $220 \text{ }^\circ\text{C}$ for 30 min, and incubated at $290 \text{ }^\circ\text{C}$ for 15 min. A resultant black suspension was formed, from which the desired Pd-Ni-P NPs were collected by centrifugation.

3. RESULTS AND DISCUSSION

TEM shows the monodisperse NPs were formed with a size of 3 nm (Figure 1a). Energy-dispersive X-ray (EDX) demonstrated the existence of elemental Pd, Ni, and P (Figure S1). Notably, the quick reduction by strong reductant BTB did not lead to the crystallization of Pd or Ni-P phases. HRTEM (Figure 1b) and XRD pattern (Figure 2e) indicated an amorphous structure of the NPs was formed. Except for the addition of TOPO, the combination of Pd, Ni, and P were essential for the formation of amorphous composite, as Pd-P NPs were fabricated with a crystalline morphology in the same conditions.[15]

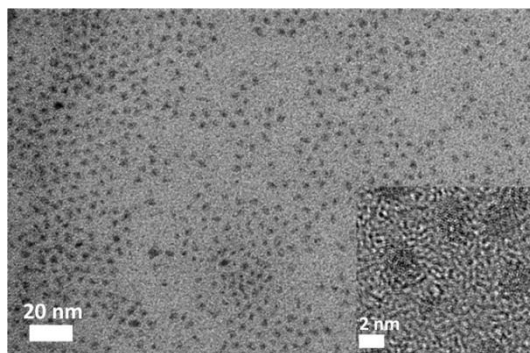


Figure 1. TEM and HRTEM (inset) images of the as synthesized 3 nm amorphous Pd-Ni-P NPs.

Next, Vulcan XC-72 and multi-walled CNTs were employed respectively as the carriers of the NPs. The particles and two kinds of carbons were mixed with a weight ratio of 40/60 respectively in

hexane, dried, and annealed under 300 °C or 400 °C to form the amorphous (Figures 2a and 2c) or crystalline catalysts (Figures 2b and 2d), respectively. Inductively coupled plasma mass spectrometry (ICP-MS) determined the compositions of the catalysts as Pd₂₅Ni₂₅P₅₀, which is accordant with the mole ratio of Pa(acac)₂ to Ni(acac)₂. From TEM (Figure 2a-d), the size of NPs barely changed after the calcinations. HRTEM (Figures S4 and S5) and XRD patterns illustrated the two different morphologies (Figures 2e and 2f). This result demonstrated the crystallization temperature of Pd₂₅Ni₂₅P₅₀ NPs was between 300 °C and 400 °C, which is in accordance with that of Pd-Ni-P bulk metallic glass[24-25]. For comparison, 3 nm Pd NPs and Pd₅₀Ni₅₀ NPs were also prepared (see the Supporting Information, SI).

The catalytic properties of the materials were examined in MOR and monitored by cyclic voltammetry (CV) performed with a three-electrode setup. The CV experiments were performed in 0.5 M KOH (aq.) containing 1.0 M methanol (see details in SI). In Figure 3a, Pd₂₅Ni₂₅P₅₀/C showed the highest specific activity (normalized by the electrochemical surface area of Pd) of 0.51 mA/cm²_{Pd} compared with the home-made Pd₅₀Ni₅₀/C and Pd/C, which is accordant with the previous result.[24] Notably, Pd₂₅Ni₂₅P₅₀/CNTs achieved much higher current density of 0.91 mA/cm²_{Pd}. From Figure 3b, we can see the specific activity of Pd₂₅Ni₂₅P₅₀/CNTs was 1.8 times as high as that of Pd₂₅Ni₂₅P₅₀/C. The high MOR activity of Pd-Ni-P/CNTs may arise from two factors: (i) CNTs have large surface areas and are able to absorb more methanol, facilitating its activation by the adjacent Pd-Ni-P NPs; (ii) CNTs are highly conductive and can promote electron transfer across the CNTs-electrode and CNTs-metal interfaces to reduce MOR overpotential. [26-27]

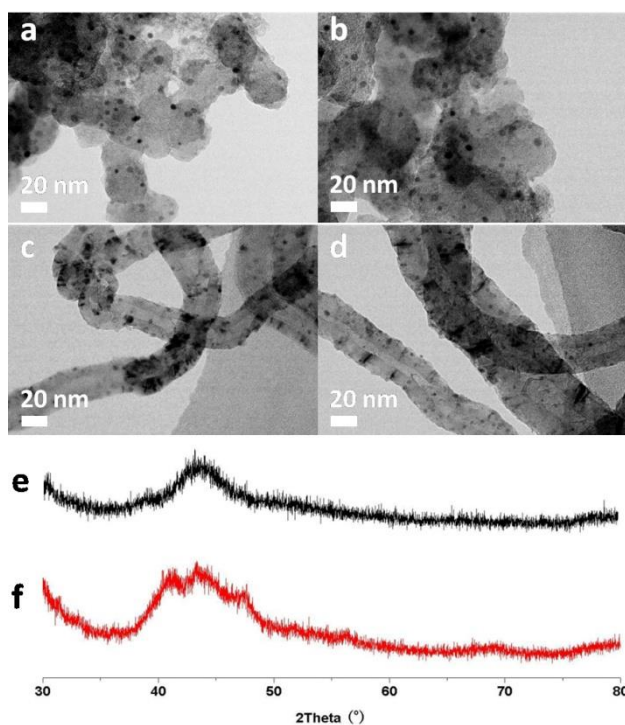


Figure 2. TEM images of Pd₂₅Ni₂₅P₅₀/C (a, amorphous and b, crystalline) and Pd₂₅Ni₂₅P₅₀/CNTs (c, amorphous and d, crystalline); XRD patterns of Pd-Ni-P/C (e, amorphous and f, crystalline).

The unique catalytic property of amorphous Pd-Ni-P NPs was further confirmed by comparison with its crystalline counterpart. The latter was obtained by simply annealing Pd-Ni-P NPs under 400 °C. Although with the same compositions, the amorphous catalyst presented a superior performance both in activity and anti-poison property (Figure 3c). The specific activity 0.91 mA/cm²_{Pd} was around 1.3 times higher than that of crystalline ones (0.73 mA/cm²_{Pd}). Moreover, the I_f/I_b (the ratio between forward and backward peak current) value of 1.9 was also much higher than that from crystallized counterpart ($I_f/I_b = 1.1$) and comparable with many other well modified Pd electro-catalysts.[28-30] It indicated the amorphous Pd-Ni-P NPs show better tolerance of the anode against the poisoning species, namely MOR intermediates (e.g. CO and HCOO⁻). It may stem from the random arrangement of Pd, Ni, and P atoms and the electron deficiency of Pd (*vide infra*). In Figure 3d, a commercial Pd supported on carbon matrix (designated Ald Pd/C, Figure S6) showed a lower activity of 0.56 mA/cm²_{Pd} in comparison with Pd-Ni-P/CNTs.

The electron-deficiency on Pd in Pd-Ni-P alloy was observed by XPS. The binding energy (BE) of Pd 3d_{5/2} in Pd-Ni-P/C (337.8 eV, Figure 4c) exhibits a large positive shift (more than 2.0 eV) compared with both two values in Pd-Ni (335.4 eV, Figure 4b) and Pd NPs (335.0 eV, Figure 4a). The positive charged Pd in the Pd-Ni-P system contributed to the higher catalytic efficiency probably caused by the decreased adsorption energy of MOR intermediates.[9,31]

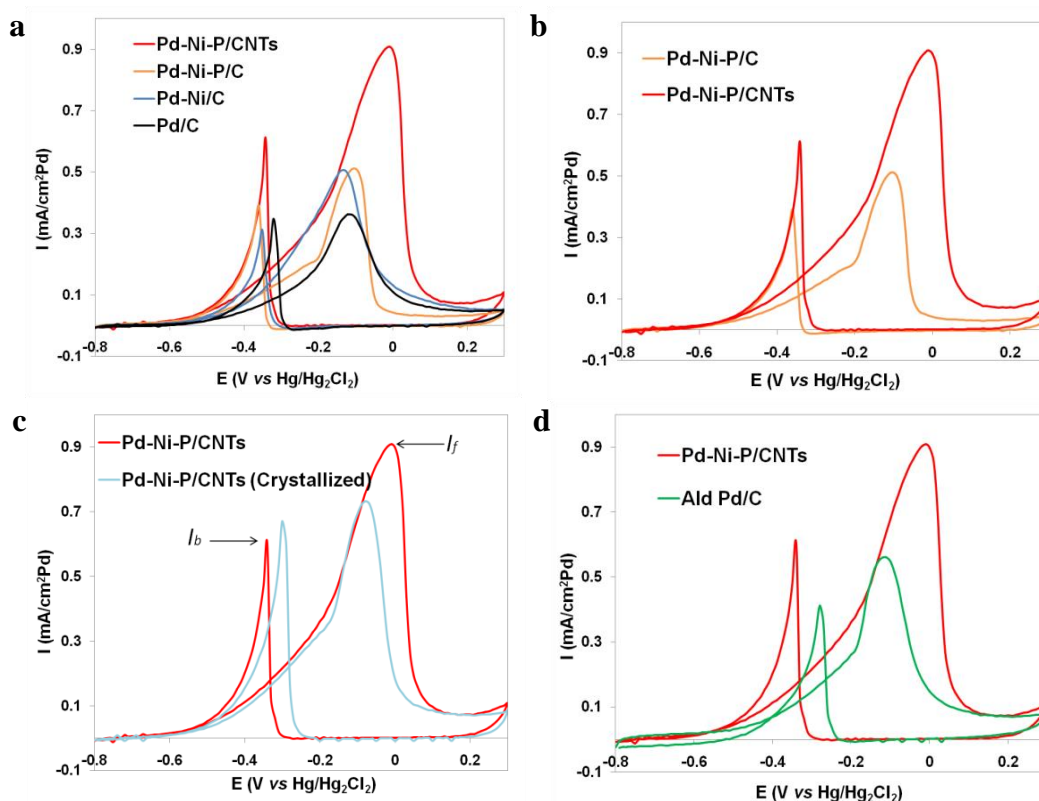


Figure 3. Current density–potential curves of the cyclic CV test to compare the catalytic activities of different Pd-based catalysts in MOR.

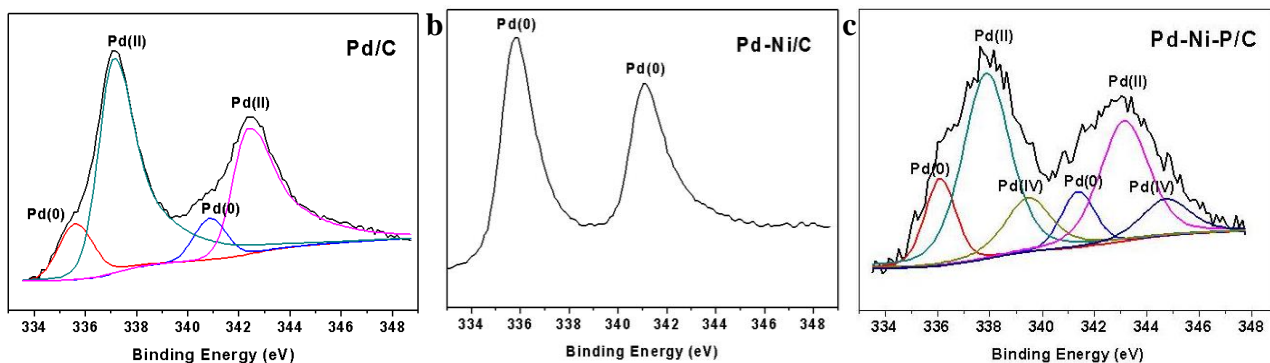


Figure 4. XPS spectra of different Pd-based NPs supported on activated carbon. The binding energy of Pd(3d) was illustrated.

4. CONCLUSIONS

In summary, we have succeeded to fabricate ultrafine amorphous Pd-Ni-P NPs with an average size of 3 nm. The Pd-Ni-P composite show superior catalysis and poison resistance in MOR compared with Pd, Pd-Ni, and its crystalline counterpart. Notably, CNTs were demonstrated to be a more efficient support, using which the resulting specific activity was much higher than that using activated carbon. This synthesis method was expected to be applied to produce other metal-P nanomaterials with ultrafine size, and the combination of amorphous Pd-Ni-P with a π -conjugated carbon would enlighten the design of other efficient catalysts.

SUPPLEMENTARY INFORMATION:

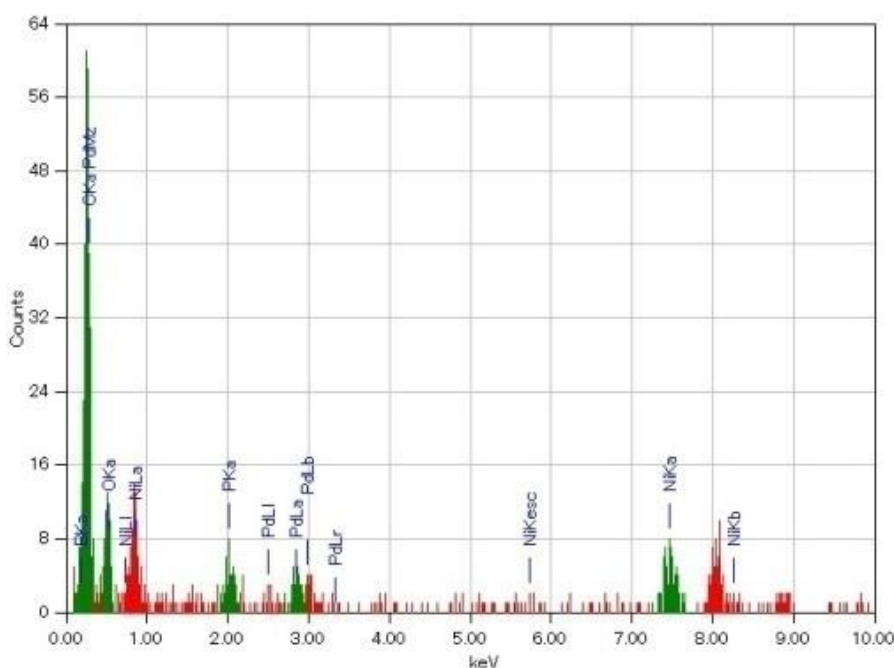


Figure S1 Energy-dispersive X-ray (EDX) analysis of 3 nm Pd-Ni-P NPs.

Fabrication of Pd/C. The coated Pd NPs were fabricated according to the previous method reported by Hyeon.[32] For the fabrication of Pd/C: In a round-bottom flask, a suspension of activated carbon in toluene (70 mg in 140 mL) was under ultrasonic for 25 min, to which a solution of as-synthesized Pd NPs in toluene (30 mg in 120 mL) was added. After that, the mixture went through ultrasonic for another 25 min. After evaporated to remove toluene, the mixture was calcined at 300 °C under nitrogen gas for 2 h.

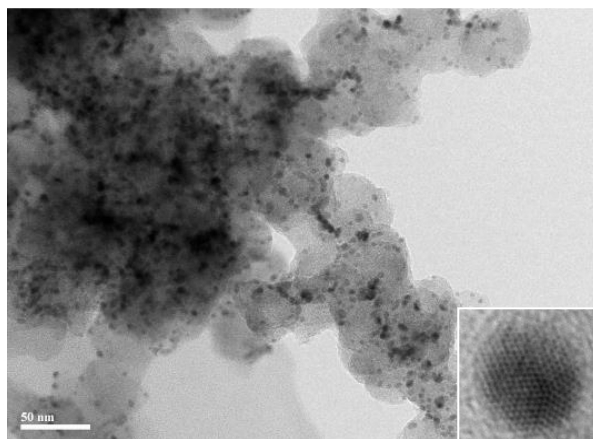


Figure S2 TEM and HRTEM (inset) images of 3 nm Pd /C.

Fabrication of Pd-Ni/C. The coated Pd-Ni alloy NPs were fabricated according to the previous method reported by Han.[33] In a three-neck flask with reflux apparatus, a mixture of Pd(acac)₂ (0.1 mmol), Ni(acac)₂ (0.1 mmol) and 0.6 mmol of BTB were dissolved in a mixed solvent of OA (0.4 mL) and OLA (20 mL) at room temperature, and the mixture was stirred for 30 min under a nitrogen flow. Then, it was heated to 270 °C with a heating rate of 15 °C min⁻¹, and kept at that temperature for 40 min. After the reactants were cooled down to room temperature, added 40 mL of ethanol. Centrifugation (10000 rpm) for 8 min gave Pd-Ni-P NPs coated by OLA as the precipitation, which was washed with ethanol (30 mL) carefully. The resulting material was disperse and kept in toluene. For the fabrication of Pd-Ni/C: In a round-bottom flask, a suspension of activated carbon in toluene (70 mg in 140 mL) was under ultrasonic for 25 min, to which a solution of as-synthesized Pd-Ni NPs in toluene (30 mg in 120 mL) was added. After that, the mixture went through ultrasonic for another 25 min. After evaporated to remove toluene, the mixture was calcined at 300 °C under nitrogen gas for 2 h.

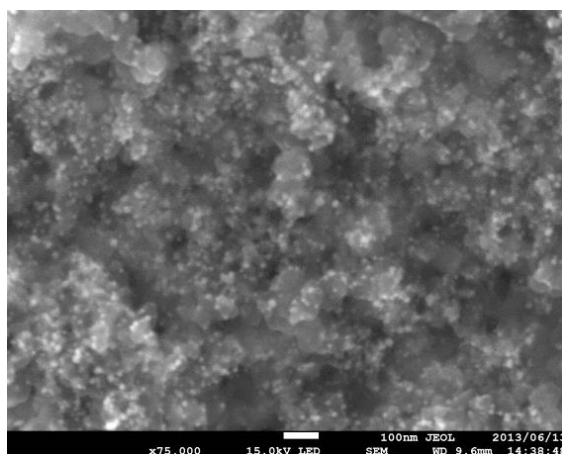


Figure S3 SEM image of Pd-Ni/C catalyst.

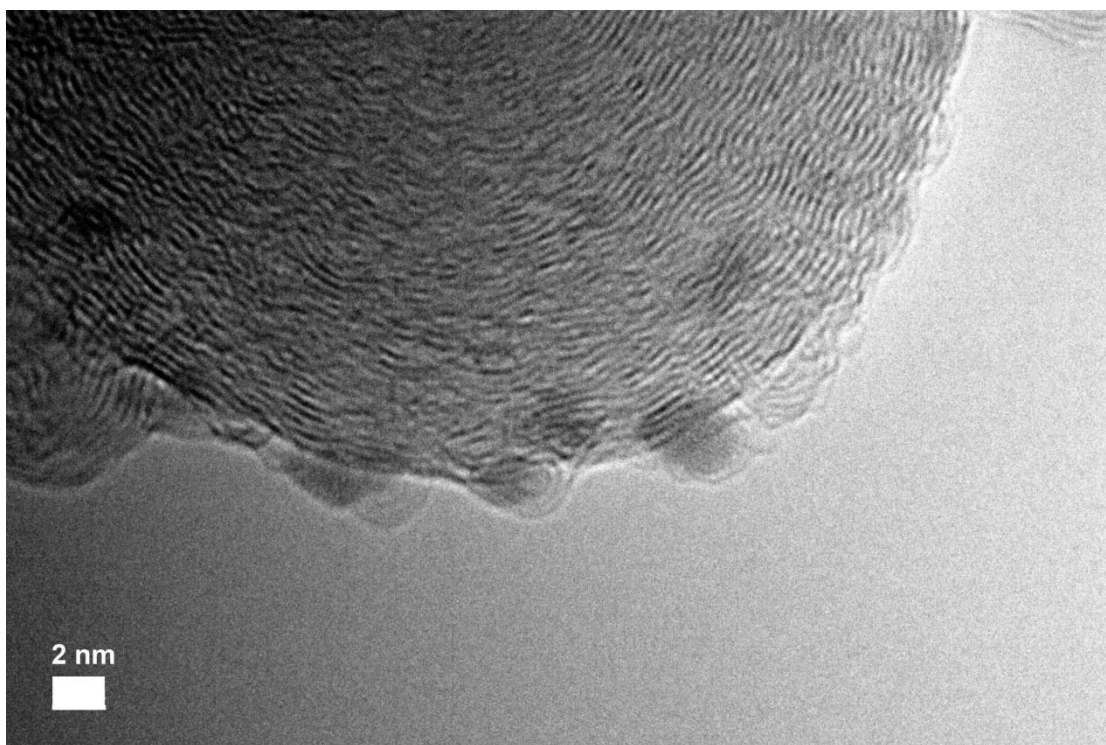


Figure S4 HRTEM image of amorphous Pd-Ni-P/C catalyst.

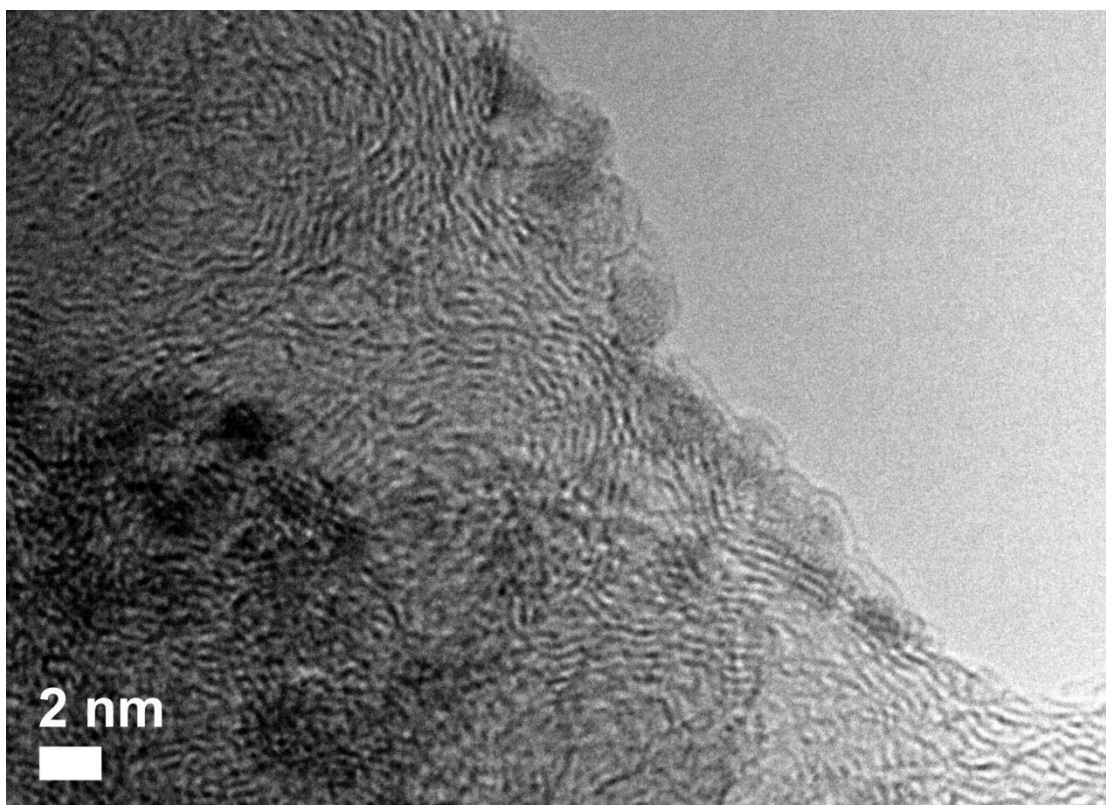


Figure S5 HRTEM image of crystalline Pd-Ni-P/C catalyst.

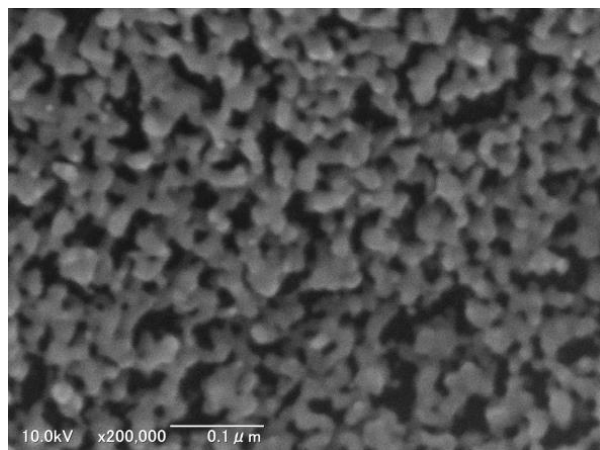


Figure S6 SEM image of Pd/C catalyst purchased from Sigma-Aldrich Co.

ACKNOWLEDGEMENT

This work was supported by Fundamental Research Funds for the Central Universities (no. 2015XKMS048), the Natural Science Foundation of Jiangsu Province (no. BK20160254), and a Project Funded by the Priority Academic Program Development of Jiangsu Higher Education Institutions.

References

1. L. Yin, J. Liebscher, *Chem. Rev.* 107 (2007) 133.
2. Á. Molnár, *Chem. Rev.* 111 (2011) 2251.
3. C. Li, Y. Su, X. Lv, H. Shi, X. Yang, Y. Wang, *Mater. Lett.* 69 (2012) 92.
4. D. Teschner, J. Borsodi, A. Wootsch, Z. Révay, M. Hävecker, A. Knop-Gericke, S. D. Jackson, R. Schlögl, *Science* 320 (2008) 86.
5. W. -J. Yoo, H. Miyamura, S. Kobayashi, *J. Am. Chem. Soc.* 133 (2011) 3095.
6. V. Mazumder, S. Sun, *J. Am. Chem. Soc.* 131 (2009) 4588.
7. V. Mazumder, M. Chi, M. N. Mankin, Y. Liu, O. Metin, D. Sun, K. L. More, S. Sun, *Nano Lett.* 12 (2012) 1102.
8. For reviews of palladium-based electrocatalysts for alcohol oxidation, see: C. Bianchini, P. K. Shen, *Chem. Rev.* 109 (2009) 4183.
9. M. Yin, Q. Li, J. O. Jensen, Y. Huang, L. N. Cleemann, N. J. Bjerrum, W. Xing, *J. Power Sources* 219 (2012) 106.
10. Y. Xu, R. Xu, J. Cui, Y. Liu, B. Zhang, *Chem. Commun.* 48 (2012) 3881.
11. Z. Niu, Q. M. Gong, H. Rong, Y. Li, *Angew. Chem., Int. Ed.* 50 (2011) 6315.
12. L. X. Ding, A. L. Wang, G. R. Li, Z. Q. Liu, W. X. Zhao, C. Y. Su, Y. X. Tong, *J. Am. Chem. Soc.* 134 (2012) 5730.
13. X. Xue, J. Ge, C. Liu, W. Xing, T. Lu, *Electrochem. Commun.* 8 (2006) 1280.
14. X. Xue, J. Ge, T. Tian, C. Liu, W. Xing, T. Lu, *J. Power Sources* 172 (2007) 560.
15. M. Zhao, *Chem. Asian J.* 11 (2016) 461.
16. J. Chang, L. Feng, C. Liu, W. Xing, X. Hu, *Angew. Chem., Int. Ed.* 53 (2014) 122.
17. J. Zhang, Y. Xu, B. Zhang, *Chem. Commun.* 50 (2014) 13451.
18. J. J. Vilatelal, R. Marcilla, *Chem. Mater.* 27 (2015) 6901.
19. S. Sarkar, M. L. Moser, X. Tian, X. Zhang, Y. F. Al-Hadeethi, R. C. Haddon, *Chem. Mater.* 26 (2014) 184.
20. N. Kakati, J. Maiti, S. H. Lee, S. H. Jee, B. Viswanathan, Y. S. Yoon, *Chem. Rev.* 114 (2014)

12397.

21. M. Liu, R. Zhang, W. Chen, *Chem. Rev.* 114 (2014) 5117.
22. Y. Zhou, *et al. J. Mater. Chem. A* 3 (2015) 8459.
23. G.-P. Jin, R. Baron, N. V. Rees, L. Xiao, R. G. Compton, *New J. Chem.* 33 (2009) 107.
24. M. Zhao, K. Abe, S. Yamaura, Y. Yamamoto, N. Asao, *Chem. Mater.* 26 (2014) 1056.
25. T. Takeuchi, D. Fukamaki, H. Miyazaki, K. Soda, M. Hasegawa, H. Sato, U. Mizutani, T. Ito, S. Kimura, *Mater. Trans.* 48 (2007) 1292.
26. Q. Dong, Y. Li, L. Zhu, T. Ma, C. Guo, *Int. J. Electrochem. Sci.* 8 (2013) 8191.
27. T. Jin, S. Guo, J. Zuo, S. Sun, *Nanoscale*, 5 (2013) 160.
28. F. Miao, B. Tao, L. Sun, T. Liu, J. You, L. Wang, P. K. Chu, *J. Power Sources* 195 (2010) 146.
29. A.-X. Yin, X.-Q. Min, Y.-W. Zhang, C.-H. Yan, *J. Am. Chem. Soc.* 133 (2011) 3816.
30. R. K. Pandey, V. Lakshminarayanan, *J. Phys. Chem. C* 113 (2009) 21596.
31. A.-L. Wang, H. Xu, J.-X. Feng, L.-X. Ding, Y.-X. Tong, G.-R. Li, *J. Am. Chem. Soc.* 135 (2013) 10703.
32. S.-W. Kim, J. Park, Y. Jang, Y. Chung, S. Hwang, T. Hyeon, *T. Nano Lett.* 3(2003) 1289-1291.
33. K. Lee, S. W. Kang, S. -U. Lee, K. -H. Park, Y. W. Lee, S. W. Han, *ACS Appl. Mater. Interfaces* 4 (2012)4208-4214.

© 2016 The Authors. Published by ESG (www.electrochemsci.org). This article is an open access article distributed under the terms and conditions of the Creative Commons Attribution license (<http://creativecommons.org/licenses/by/4.0/>).